Polymer 51 (2010) 2455–2459

Contents lists available at ScienceDirect

Polymer

journal homepage: www.elsevier.com/locate/polymer

Polymer Communication

Visualization of nanomechanical mapping on polymer nanocomposites by AFM force measurement

Dong Wang [a], So Fujinami [a], Ken Nakajima [a], Shigeki Inukai [b], Hiroyuki Ueki [b], Akira Magario [b], Toru Noguchi [b], Morinobu Endo [c], Toshio Nishi [a,*]

[a] WPI Advanced Institute for Materials Research, Tohoku University, 2-1-1 Katahira, Aoba, Sendai 980-8577, Japan
[b] Nissin Kogyo Co., Ltd., 801 Kazawa, Toumi, Nagano 389-0514, Japan
[c] Institute of Carbon Sci. & Technol., Shinshu University, 4-17-1, Wakasato, Nagano 380-8553, Japan

ARTICLE INFO

Article history:
Received 14 January 2010
Accepted 28 March 2010
Available online 7 April 2010

Keywords:
Polymer nanocomposites
Nanomechanical mapping
Carbon nanotubes

ABSTRACT

Nanocomposite based on an elastomer, natural rubber (NR), and pristine multi-walled carbon nanotubes (MWCNT) was prepared using a two-roll mill mixer. The high shearing stress induced homogeneous dispersion of 5 phr. MWCNTs in NR matrix. A procedure based on combination of Johnson–Kendall–Robert (JKR) contact mechanics and "two-point method" together with AFM force measurements, was successfully used to visualize nanomechanical mapping on the resulting nanocomposites. Topography, elastic modulus, and adhesive energy distribution maps were obtained at the same point and at the same time in a single scan. Such maps were successfully used to identify and characterize CNTs and NR regions in nanocomposites. The intermediate modulus region formed around CNTs was investigated on the quantitative evaluation in real space and demonstrated the existence of interaction between CNTs and NR matrix.

© 2010 Elsevier Ltd. All rights reserved.

1. Introduction

Atomic force microscopy (AFM) has been widely employed to study nano-structured materials, which enables us to investigate topological and mechanical properties at the same point and at the same time [1–6]. The mechanical properties such as Young's modulus are usually calculated from AFM force-distance curves [7–10]. However, such measurement only provides mechanical information at a single point. In order to map the elastic and adhesive properties of materials with surface heterogeneity, researchers use different AFM techniques such as AFM force volume (FV) [11–13], AFM tapping mode using torsional harmonic cantilevers [14], band excitation method [15], and contact resonance based techniques [16].

In this work, using a procedure based on combination of Johnson–Kendall–Robert (JKR) [17] contact mechanics and "two-point method" [18] together with AFM force volume measurements, we successfully presented a quantitative method to obtain nanomechanical mapping on polymer nanocomposites. Using this technique, maps of elastic modulus, adhesive energy and topography can be obtained simultaneously in a single scan. In addition, a procedure to rebuild a true height image is introduced, by which the real surface topography of samples can be presented. Multi-walled carbon nanotube (MWCNT) reinforced natural rubber (NR) was selected as a model nanocomposite because the CNTs are promising fillers for elastomers to improve mechanical, electrical, and thermal properties [19–22]. Our technique is promising in identifying the composition and better understanding the relationship between structure-properties of polymer nano-alloys and polymer based nanocomposites.

2. Experimental

Natural rubber (NR) used in this study was a Standard Malaysian Rubber Constant with Viscosity 60 (SMR CV60). MWCNTs with purity greater than 95% and average diameter of about 13 nm, were obtained from ILJIN Nanotech Co. Ltd. The CNTs were used as received. The NR containing 5 phr (NR5) CNTs nanocomposites was prepared as follows [23]: on a six-inch two-roll mill, the respective NR was placed and rolled upon themselves. Then, the required amounts of CNTs and cross-linking agent were added and mixed with the NR. With the mixtures temporarily removed, the nip was tightened to 0.2 mm in order to provide the compound with an extremely large shearing force. The resulted compounds were sheeted into slabs of 1.2 mm and cured by compression moulding at 175 °C for 20 min. The sheet sample was then cut by a Leica EM FC6

* Corresponding author. Tel.: +81 22 2175928.
E-mail address: nishi.toshio@wpi-aimr.tohoku.ac.jp (T. Nishi).

0032-3861/$ – see front matter © 2010 Elsevier Ltd. All rights reserved.
doi:10.1016/j.polymer.2010.03.052

ultramicrotome at −180 °C to obtain a flat surface. Force Volume (FV) experiments were performed using a commercial AFM system (Multimode series with a NanoScope V controller) under ambient condition. In the FV-mode, force curves were collected over randomly selected surface areas at a resolution of 128 × 128 pixels (16 384 force-distance curves). The cantilevers used were ORC8-10 (Veecoprobes, USA) whose nominal spring constant is 0.38 N/m. Actual spring constant was measured by thermal tune method with the value of spring constant 0.475 ± 0.003 N/m. The calibrated deflection sensitivity with a hard metal surface was used in the following analyses.

The obtained force-distance curves were analyzed using JKR contact mechanics. The theory is expressed by the following two equations:

$$a^3 = \frac{R}{K}\left(F + 3\pi WR + \sqrt{6\pi WRF + (3\pi WR)^2}\right) \quad (1)$$

$$\delta = \frac{a^2}{3R} + \frac{2F}{3aK} \quad (2)$$

where α, R, and W are the contact radius, the tip radius, and the adhesive energy, respectively. K is the combined elastic modulus and has the relationship to Young's modulus, E, as follows,

$$K = \frac{4E}{3(1-\nu^2)} \quad (3)$$

where ν is the Poisson's ratio. Because the above equations are unable to be converted to a function of sample deformation δ and applied load force F (F is derived from the spring constant k and the deflection of the cantilever Δ ($F = k\Delta$), the least mean square curve-fitting is not applicable. Therefore, we apply "two-point method" proposed by Sun [18]. In this method a JKR curve is drawn so as to cross the two typical points; one point is where the attractive force and the repulsive force become equivalent, and the other is where adhesive force becomes maximum (F_1). Using these two points, JKR equations are converted to the following functions where K and w are explicitly represented:

$$K = \frac{1.27F_1}{\sqrt{R(\delta_0 - \delta_1)^3}} \quad (4)$$

$$W = -\frac{2F_1}{3\pi R} \quad (5)$$

Thus, equations (3)–(5) give K and W from a force-distance curve. Supplementary data gave the detailed analysis procedures.

3. Results and discussion

Fig. 1 firstly shows a TEM image of the NR5 nanocomposites prepared by open roll mill mixer. The TEM experiments were carried out on a JEM-2200FS instrument operated at 200 kV. It can be seen that the unmodified CNTs are well dispersed in the NR matrix at 5 phr loading. The homogeneous dispersion of the CNTs can be attributed to the high shear stress exerted during mixing. The compound gets very distorted by the large shearing force when it passes the roll, but the rubber's recovery force occurs immediately after passing through the roll. By this plastic kneading of repeated distortion and recovery, it is thought that CNTs are taken from the cohesive group, thread by thread, and then are homogenously dispersed. Using an ultrahigh-shear processing extruder, Shimizu also prepared unmodified MWCNTs/polymer nanocomposites with homogeneous dispersion, such as poly[styrene-b-(ethylene-co-butylene)-b-styrene] triblock copolymer (SEBS), poly(vinylidene fluoride) (PVDF), and poly(styrene-b-butadiene-co-butylene-b-styrene) (SBBS) nanocomposites [24–26]. The high shear stress may overwhelm the electrostatic and van der Waals interactions between the nanotubes and peel each nanotube apart.

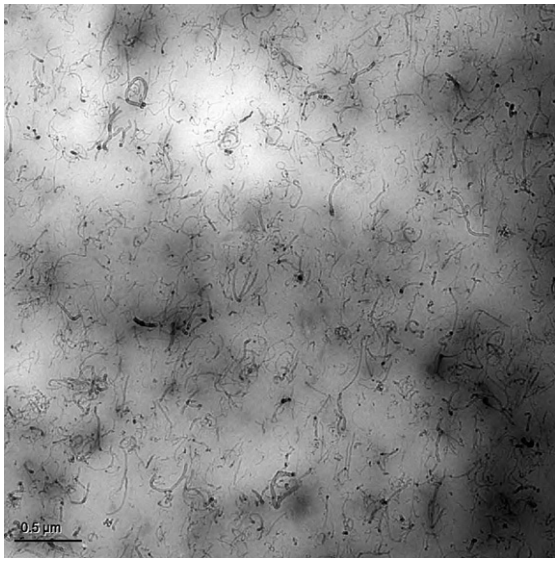

Fig. 1. TEM images of NR5 nanocomposites. Scale bar is 0.5 μm.

Fig. 2a shows the tapping mode height image and Fig. 2b–d gives the generated apparent height, sample deformation, and true height images obtained by nanomechanical mapping technique. The apparent height image is obtained directly from the FV mode, where the trigger threshold is set to 2.4 nN. The same as TEM result, tapping mode height and apparent height images also show that CNTs are dispersed uniformly throughout the nanocomposite. In our tapping mode experiment, the calculated tapping force is about 0.5–1 nN, is lower than the trigger threshold (2.4 nN). It indicates that the tapping mode height images should show lower deformation than FV apparent height image, which is demonstrated by the section analysis showed in Fig. 3S (Supplementary data). Even though, both the tapping mode height and apparent height images contain artifacts due to the very low elastic modulus of NR matrix. In this work, however, we reconstructed the true height image by superimposition of the FV apparent height and sample deformation images. As shown in Fig. 2d, the true height image shows real surface topography of NR5 sample. The weaker contrast for true height image is due to the larger compensation of deformation at NR region. Although the reconstructed true height images do not indicate much more information, it is a real topographic image free from the effect of sample deformation.

Fig. 3 shows simultaneously generated maps of the combined elastic modulus and adhesive energy of NR5 nanocomposites. By comparing the deformation (Fig. 2c), elastic modulus, and adhesive energy images, several interesting structures are observed. Two typical structures are selectively marked by two ellipses and a rectangle, respectively. Corresponding to the deformation image, the blue fiber-like structure marked by the ellipse in the modulus image represents smaller deformation, higher elastic modulus (Fig. 3a), and lower adhesive energy (Fig. 3b). Such structures are possibly assigned to CNTs. The light red and light green area marked by the rectangle (Fig. 3a) shows larger deformation, lower elastic modulus, and higher adhesive energy. Such area is possibly assigned to NR matrix. To further confirm the above conclusions, the details of elastic modulus image with 500 nm scan size are

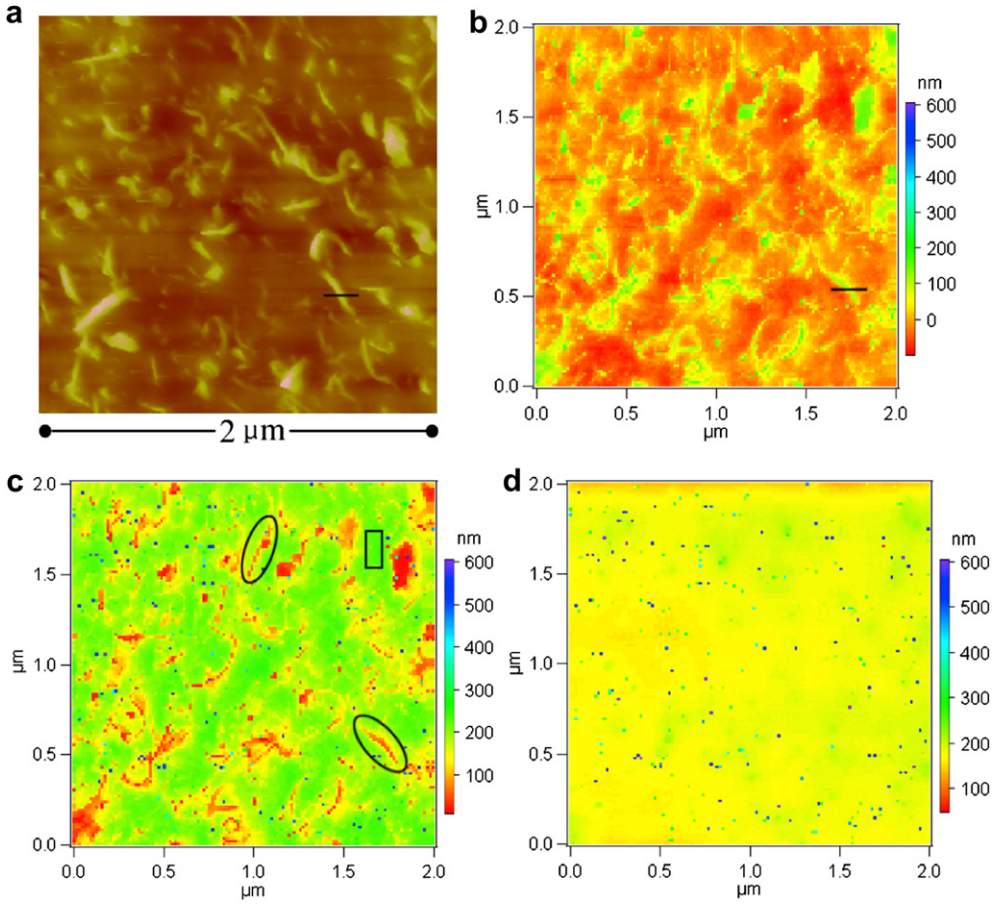

Fig. 2. AFM images of NR5 sample. (a) tapping mode height image obtained using light tapping, (b) apparent height image, (c) deformation image, and (d) true height image. Scan size is 2 μm.

investigated. As shown in Fig. 4a, the distribution of elastic modulus is divided into two typical regions: two representative points are indicated by open circles and the corresponding force-deformation curves are shown in Fig. 4b–d. The curve-fitting against JKR contact is also superimposed in each case. Firstly, the results show that JKR analysis on withdrawing process is fairly fitted. The elastic modulus in Fig. 4b is 3.5 ± 1.5 MPa, typical for a NR. The elastic modulus is 12.0 ± 1.8 MPa in Fig. 4d. Although it is far lower than the typical value of CNTs, we attribute this region as a stiff CNTs region. One possible reason for the low elastic modulus of CNTs is that the rubber surrounding CNTs is deformed. In this case, it is very difficult to know real mechanical properties of stiff materials floating on a soft material. (For interpretation of the references to colour in this text, the reader is referred to the web version of this article).

In addition to CNTs and NR regions, we also find another region, intermediate modulus region formed around CNTs. As shown in Fig. 4c, the elastic modulus of this region is 6.1 ± 0.8 MPa, stiffer than NR region but softer than CNTs region. It is impossible to

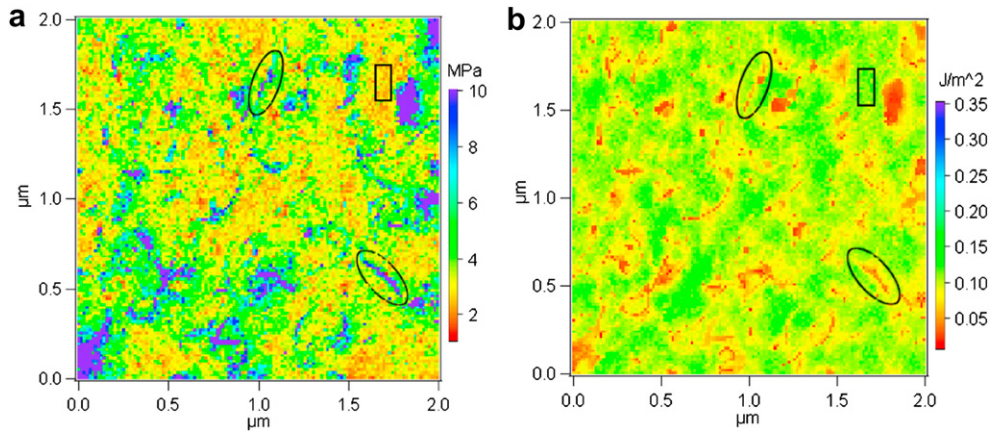

Fig. 3. Elastic modulus distribution image (a) and adhesive energy distribution image (b) of NR5 nanocomposites. Scan size is 2 μm.

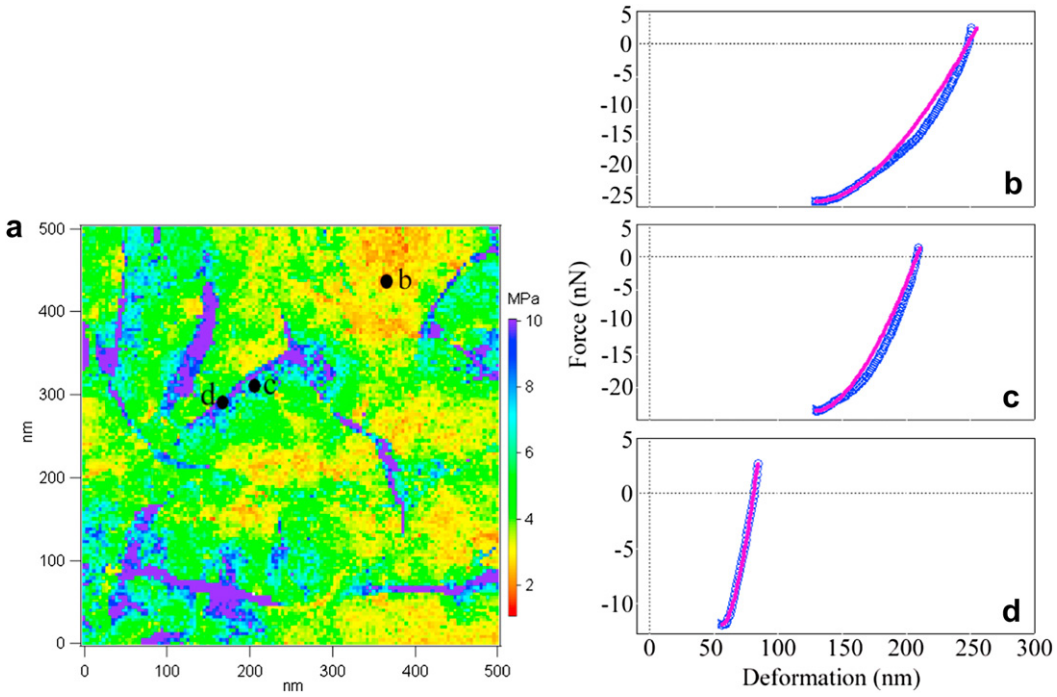

Fig. 4. Magnified elastic modulus image (a) and force-deformation curves of local points indicated by open circles in (a). The curve-fitting against JKR contact was superimposed on each curve. (b) NR region, 3.5 ± 1.5 MPa, (c) intermediate modulus region, 6.1 ± 0.8 MPa, and (d) CNT region, 12.0 ± 1.8 MPa.

explain the results by simply considering compositions. We name this as intermediate modulus region. By pullout of CNTs from polyethylene–butene film, Barber also observed the regions had anomalously high shear strength [27]. In MWCNTs/polycarbonate composites, both Ding [28] and Pötschke [29] observed thick (tens of nm) layers of polymer coating CNTs. This indicates that a layer with high shear strength is formed. In case of CNTs/NR nanocomposites, the intermediate modulus region resulted from (i) the interactions of electrostatic and van der Waals result in the limited motions of the NR molecule close to the CNTs and (ii) stress/deformation arise from the mismatch in the coefficients of thermal expansion between CNTs and the NR has been widely investigated [19–22]. Although a number of studies suggest that interactions with CNTs could result in a region around of polymer with morphology and properties different from the bulk [19–22], this paper would be the first report to quantitatively evaluate the intermediate modulus regions in real space.

Deformation and adhesive energy mapping also lead to the same conclusion as the elastic modulus studies. Thus, we may conclude that our reconstruction procedure is valid and that the elastic modulus and adhesive energy mapping represent the real topographic features. Using this technique, we visualized the nanomechanical mapping of CNTs/NR nanocomposites.

4. Conclusions

Well-dispersed CNTs/elastomer nanocomposite was prepared by open roll mill mixer with high shearing stress. Nanomechanical mapping of such prepared nanocomposites was visualized by the combination of JKR and “two-point method” analysis together with force mapping measurements. We obtained the topography, elastic modulus, and adhesive energy maps at the same point and at the same time in a single scan. Such maps were successfully used to identify and characterize CNTs and NR regions in nanocomposites in which the material properties of different compositions were separately visualized. The calculated Young’s modulus is about 3.5 ± 1.5 MPa for soft NR matrix; 12.0 ± 1.8 MPa for hard CNTs. The Young’s modulus value of soft NR component agrees well with bulk viscoelastic properties, while the value of hard CNTs shows a dramatic decrease in stiffness. The intermediate modulus region formed around CNTs was investigated on the quantitative evaluation in real space. These results will be useful to study polymer nano-alloys and polymer based nanocomposites.

Acknowledgment

This work was supported by the New Energy and Industrial Technology Development Organization (NEDO) under the Ministry of Economy, Trade, Industry (METI) in Japan.

Appendix. Supplementary data

Supplementary data associated with this article can be found in the online version at doi: 10.1016/j.polymer.2010.03.052.

References

[1] Butt HJ, Cappella B, Kappl M. Surf Sci Rep 2005;59:1–151.
[2] Huey BD. Annu Rev Mater 2007;37:351–85.
[3] Reynaud C, Sommer F, Quet C, Bounia NEL, Duc TM. Surf Interface Anal 2000;30:185–9.
[4] Kaliappan SK, Cappella B. Polymer 2005;46:11416–23.
[5] Song J, Tranchida D, Vancso GJ. Macromolecules 2008;41:6757–62.
[6] Raghavan D, Gu X, Nguyen T, VanLandingham M, Karim A. Macromolecules 2000;33:2573–83.
[7] Cappella B, Dietler G. Surf Sci Rep 1999;34:1–104.
[8] Sun YJ, Akhremitchev B, Walker GC. Langmuir 2004;20:5837–45.
[9] Du BY, Tsui OKC, Zhang QL, He TB. Langmuir 2001;17:3286–91.
[10] Achalla P, McCormick J, Hodge T, Moreland C, Esnault P, Karim A, et al. J Polym Sci Part B Polym Phys 2006;44:492–503.
[11] Schönherr H, Hruska Z, Vancso GJ. Macromolecules 2000;33:4532–7.
[12] Nishi T, Nukaga H, Fujinami S, Nakajima K. Chin J Polym Sci 2007;25:35–41.
[13] Nagai S, Fujinami S, Nakajima K, Nishi T. Compos Interfac 2009;16:13–25.
[14] Sahin O, Erina N. Nanotechnology 2008;19:445717.

[15] Jesse S, Kalinin SV, Proksch R, Baddorf AP, Rodriguez BJ. Nanotechnology 2007;18:435503.
[16] Stan G, Cook RF. Nanotechnology 2008;19:235701.
[17] Johnson KL, Kendall K, Roberts AD. Proc R Soc London Ser A 1971;324:301–13.
[18] Sun Y, Walker GC. Langmuir 2004;20:5837–45.
[19] Moniruzzaman M, Winey KI. Macromolecules 2006;39:5194–205.
[20] Coleman JN, Khan U, Blau WJ, Gun'ko YK. Carbon 2006;44:1624–52.
[21] Endo M, Noguchi T, Ito M, Takeuchi K, Hayashi T, Kim YA, et al. Adv Funct Mater 2008;18:3403–9.
[22] Bokobza L. Polymer 2007;48:4907–20.
[23] Noguchi T, Inukai S, Uekii H, Magario A, Endo M. SAE International; 2009. 2009-01-0606.
[24] Li YJ, Shimizu H. Macromolecules 2009;42:2587–93.
[25] Chen JX, Li YJ, Shimizu H. Carbon 2007;45:2334–40.
[26] Li YJ, Shimizu H. Polymer 2007;48:2203–7.
[27] Barber AH, Cohen SR, Wagner HD. Appl Phys Lett 2003;82:4140–2.
[28] Ding W, Eitan A, Fisher FT, Chen X, Dikin DA, Andrews R, et al. Nano Lett 2003;3:1593–7.
[29] Pötschke P, Fornes TD, Paul DR. Polymer 2002;43:3247–55.